External-Field-Robust Stochastic Magnetic Tunnel Junctions Using a Free Layer with Synthetic Antiferromagnetic Coupling

Keito Kobayashi,[1,2] Keisuke Hayakawa,[1,2] Junta Igarashi,[1] William A. Borders,[1] Shun Kanai,[1,2,3,4,5,6,*] Hideo Ohno,[1,2,5,6,7] and Shunsuke Fukami[1,2,5,6,7,8]

[1] *Laboratory for Nanoelectronics and Spintronics, Research Institute of Electrical Communication, Tohoku University, Sendai 980-8577, Japan*

[2] *Graduate School of Engineering, Tohoku University, Sendai 980-0845, Japan*

[3] *PRESTO, Japan Science and Technology Agency, Saitama 332-0012, Japan*

[4] *Division for the Establishment of Frontier Sciences, Tohoku University, Sendai 980-8577, Japan*

[5] *Center for Science and Innovation in Spintronics, Tohoku University, Sendai 980-8577, Japan*

[6] *WPI-Advanced Institute for Materials Research, Tohoku University, Sendai 980-8577, Japan*

[7] *Center for Innovative Integrated Electronic Systems, Tohoku University, Sendai 980-0845, Japan*

[8] *Inamori Research Institute for Science, Kyoto 600-8411, Japan*

(Received 11 June 2022; revised 2 September 2022; accepted 11 October 2022; published 29 November 2022)

The stochastic magnetic tunnel junction (MTJ), the resistance of which fluctuates in time between low and high states under thermal fluctuation, is expected to serve as a key element in probabilistic computers. For reliable operation and versatile application, one needs to address the challenge that the relaxation time in each state should be virtually independent of external magnetic fields in the range of, for example, several mT. In this research, we fabricate in-plane easy-axis elliptical stochastic MTJs with a synthetic antiferromagnetic (SAF) free layer and examine the robustness of their properties against external fields while comparing them with stochastic MTJs with a conventional single ferromagnetic structure. We show that the MTJ with a SAF free layer shows more robust relaxation times against fields applied along the easy- and hard-axis directions. The results are reproduced with a macrospin simulation, from which design guidelines for robust stochastic MTJs targeting probabilistic computers are discussed.

DOI: 10.1103/PhysRevApplied.18.054085

I. INTRODUCTION

Stochastic spintronic devices, in which thermal fluctuations randomly switch the magnetization configuration, are a promising building block for unconventional computing schemes that utilize stochasticity [1–13]. Among the devices, stochastic magnetic tunnel junctions (MTJs) attract significant attention because of their high compatibility with magnetic random-access memory technology. Accordingly, a number of experimental and theoretical studies have been carried out to characterize and enhance the performance of stochastic MTJs [14–28]. In particular, a theoretical study revealed that in-plane easy-axis MTJs with sizable negative perpendicular anisotropy are favorable for achieving a fast operation, i.e., a short relaxation time, which is necessary to enhance the computation speed of the probabilistic computer [22,23], and short relaxation times down to a few nanoseconds have been demonstrated [23,24].

For practical applications, whether unintentionally or through deliberate attacks, finite external magnetic fields applied to the devices are anticipated to compromise the integrity of operation, requiring investigation into the critical properties of the stochastic MTJs that produce robustness against such external magnetic fields. The geometric mean relaxation time, an essential index of the stochastic MTJ, is, in principle, insensitive to magnetic fields [23,24], resulting in the fact that the time-averaged property, another important index representing the sigmoidlike response of the time-averaged resistance to external input, has been reported to vary from the fixed-0 state to the fixed-1 state with applied magnetic fields in the range of a few mT [15,18,23,26].

Here, we show an external-field-robust stochastic MTJ employing a synthetic antiferromagnetic (SAF) free layer. The SAF structure is expected to be robust against external fields due to the compensated magnetization. We measure the magnetic field dependence of the relaxation time of stochastic MTJs with the SAF free layer and compare it with MTJs with a conventional single ferromagnetic (SF) free layer [23]. Furthermore, we perform an

*skanai@tohoku.ac.jp

analytical calculation based on the magnetostatic energy as well as a numerical calculation for the dynamic process using the Landau-Lifshitz-Gilbert (LLG) equation. From these calculations, we show design guidelines for stochastic MTJs using a SAF free layer for field-robust probabilistic computers.

II. EXPERIMENT

In this section, we describe the device structures, fabrication methods, and measurement results. We show the variation of the relaxation time against in-plane external magnetic fields in the direction of the major (easy) axis (H_x) and minor (hard) axis (H_y) of the elliptical MTJs and compare the robustness of the SF and SAF structures. We note that we do not examine the effect of a perpendicular external field because it is negligibly small compared with the effective perpendicular anisotropy field (~ -1 T) of our devices.

A. Experimental setup

The stack structures investigated here are shown in Fig. 1(a); these are deposited by dc and rf magnetron sputtering on a thermally oxidized Si substrate. The stack for the SAF structure is Ta(5 nm)/Pt-Mn(20 nm)/Co(2 nm)/Ru(0.85 nm)/Co-Fe-B(2.2 nm)/MgO(1.1 nm)/Co-Fe-B(1.8 nm)/Ru(0.74 nm)/Co-Fe-B(2.1 nm)/Ta(5 nm)/Ru(5 nm). The 1.8-nm-thick and 2.1-nm-thick Co-Fe-B layers are antiferromagnetically coupled with Ru(0.74 nm) through the Ruderman-Kittel-Kasuya-Yosida (RKKY) interaction, forming a SAF free layer. Note that the thickness of the upper Co-Fe-B layer is 0.3 nm thicker than the lower one, considering a magnetically inactive "dead layer" at the interface with the adjacent Ta [29]. As a reference, we also prepare a conventional stochastic MTJ [23], where the SAF free layer is replaced with a single Co-Fe-B(2.1 nm) layer. Figure 1(b) shows a magnetization curve (M-H_x curve) of a blanket film comprising the SAF free layer [buffer/Co-Fe-B(1.8 nm)/Ru(0.74 nm)/Co-Fe-B(2.1 nm)/cap] measured with a vibrating sample magnetometer, where the sample is annealed under the conditions described below. From the saturation field shown by the dashed line, the effective magnetic field, $\mu_0 H_{\mathrm{RKKY}}$, of the RKKY interaction is determined to be about 150 mT (μ_0 is the permeability of vacuum). The stacks are processed into elliptical MTJs by electron-beam lithography and Ar-ion milling, followed by annealing at 300 °C for 2 h under an external field, $\mu_0 H_x$, of 1.2 T to fix the magnetization direction of the reference layer. The geometric average of the diameters and aspect ratio of the measured MTJs are designed to be 40–100 nm and 1.5–2.5, respectively. Figure 1(c) shows a scanning electron microscopy image of a typical MTJ with a size and aspect ratio of 67×103 nm^2 and 1.5, respectively. The ellipse's major (minor) axis is defined as the x (y) direction. Figure 1(d) shows an R-H_x curve, showing superparamagnetic behavior with zero coercive fields. The resistance area product, RA, is determined to be 17 $\Omega\mu$m^2, and the typical tunnel magnetoresistance ratio is 71%.

The random-telegraph-noise (RTN) signal under external magnetic fields is measured by an electrical circuit, as shown in Fig. 2(a). Figure 2(b) shows a RTN signal of a typical MTJ with a SAF free layer at $\mu_0 H_x = 15$ mT and source voltage of $V = 200$ mV. The transmitted voltage representing the magnetization configuration fluctuates between high and low levels, corresponding to the antiparallel (AP) and parallel (P) configurations of the MTJ. As in our previous works [22,23], we define the event time, t_{event}, as the sum of the dwell time, τ_{dwell}, and transition time, τ_{trans}, and the relaxation time, τ, as the expectation value of the event time, t_{event}, given by the Néel-Arrhenius law, $\tau = \tau_0 \exp\Delta$, where τ_0 is the attempt time and Δ is the thermal stability factor. Figure 2(d) shows the normalized number, N, of magnetization reversals from P-to-AP (left) and AP-to-P (right) configurations as a function of t_{event}. To obtain reliable statistics, we measure the RTN for a sufficiently long duration containing more than 20 000 reversals; 4 ms for the case of Fig. 2(b).

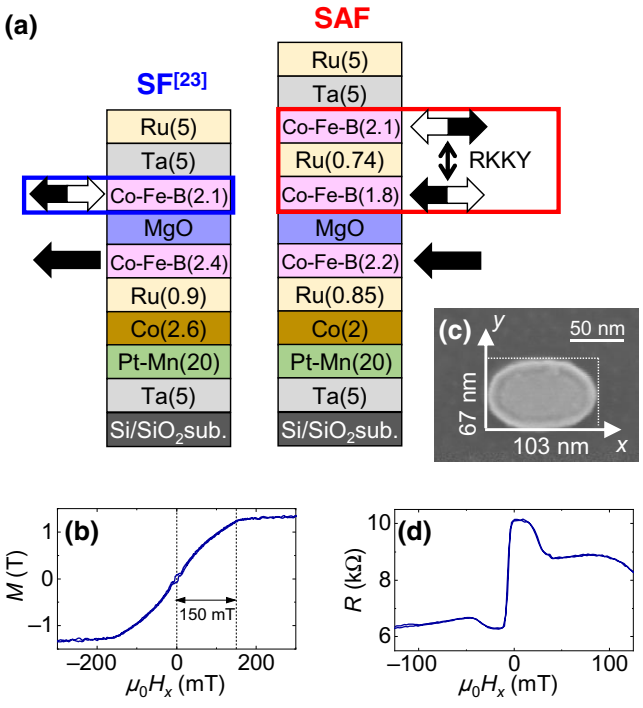

FIG. 1. (a) Stack structure of a MTJ with SF free layer and SAF free layer. Numbers in parentheses are nominal thicknesses in nm. (b) Magnetization as a function of easy-axis- (x) direction magnetic field, H_x, for a blanket film with SAF free layer. (c) Scanning electron microscope image of a MTJ and definitions of the x and y directions. (d) Resistance of a MTJ with SAF free layer as a function of H_x.

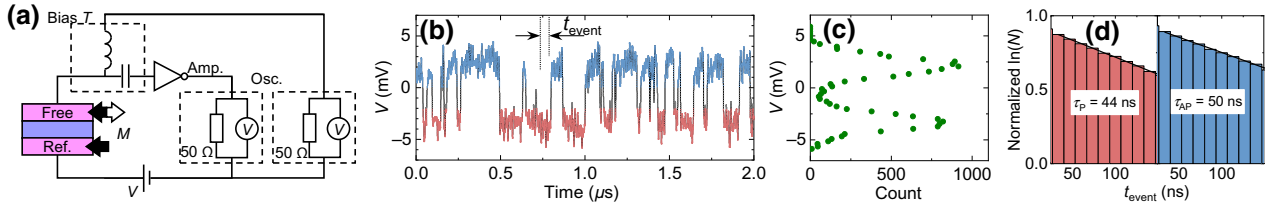

FIG. 2. (a) Electrical circuit for RTN measurements. At the oscilloscope serially connected to the high-frequency amplifier, the signal is collected with 1.3 GS/s, which is well above the inverse of the relaxation time. (b) RTN signal V of MTJ with SAF free layer measured at an easy-axis magnetic field of $\mu_0 H_x = 15$ mT. (c) Number of V. (d) Histogram of the normalized number, N, of magnetization reversals as a function of event time, t_{event}.

The obtained histogram shows a clear exponential distribution, $N(t_{event}) \propto \exp(-t_{event}/\tau)$, from which the expectation value of the event time, namely, the relaxation time,τ, is derived.

B. Easy-axis-field (H_x) dependence

First, we show the relaxation time of the P (AP) state, $\tau_{P(AP)}$, versus the in-plane easy-axis (major elliptical axis) magnetic field, H_x', in Fig. 3(a). H_x' is the net applied magnetic field in the x direction, where a shift field from the reference layer is subtracted. The red (blue) plot shows the results for the SAF (SF) structure. The two structures show comparable relaxation times on the order of 10 ns. Also, as expected, the SAF free layer is less sensitive to the magnetic field than the SF free layer. Note that the range of measured fields for the SF structure is much narrower than that for the SAF structure because the SF free layer is fixed to either of two configurations at magnetic fields above ± 1 mT. In addition, because of the slight difference in volume between the upper and lower free layers, the relaxation time of the SAF structure appears to saturate with increasing magnetic field, as shown later in Fig. 5(b) (Sec. III). The ratio of the relaxation times of the AP and P states (τ_{AP}/τ_P) against the easy-axis magnetic field is shown in Fig. 3(b). We fit an exponential function, $\tau \propto \exp(AH_x)$, to the data and obtain coefficient A [slope on the log scale, as shown in Fig. 3(b)] to be (1.81 ± 0.10) and (0.30 ± 0.03) mT^{-1} for the SF and SAF free layers, respectively, indicating an improvement of about 6 times by employing the SAF structure. We note that the residual external magnetic field dependence for the SAF free layer is likely to arise from a small uncompensated magnetic moment, as discussed in the next section. Figure 3(c) shows the averaged relaxation time, which is defined as $\tau_{av} = \sqrt{\tau_P \tau_{AP}}$ as a function of $\mu_0 H_x'$, where taking the geometric mean instead of the arithmetic mean gives the relaxation time determined by the energy barrier unperturbed by H_x [22–24]. Unlike τ_{AP}/τ_P, τ_{av} shows no apparent variation with the magnetic field, i.e., the relaxation time itself is insensitive to the external field, which is in agreement with our previous report [23]. We also note that the arithmetic mean of the relaxation time, $(\tau_P + \tau_{AP})/2$, slightly increases with $|H_x'|$, as shown in a previous paper [30].

C. Hard-axis-field (H_y) dependence

Next, we study τ_{av} against H_y. Figures 4(a) and 4(b) show τ_{av} versus H_y for MTJs with SF and SAF free layers over the $\mu_0 H_y$ range of ± 10 and ± 130 mT, respectively. The same color code as that in Fig. 3 is used. Note also that the MTJs used for Figs. 3 and 4 are different. In Fig. 4(a), τ_{av} of the SF free layer varies over 8 orders of magnitude (from 10 ns to 1 s), whereas that of the SAF free layer varies only by about 2 orders of magnitude (from 100 ns to 10 μs), indicating the 10^6 times higher robustness of the

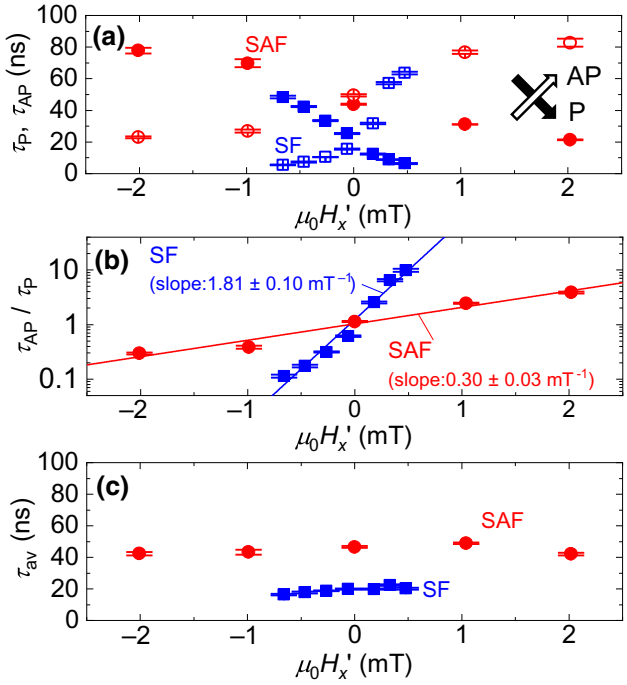

FIG. 3. (a) Relaxation time, τ_P (τ_{AP}), of the P (AP) state; (b) ratio of relaxation times, τ_{AP}/τ_P; and (c) averaged relaxation time, τ_{av}, as a function of the x-direction net magnetic field, H_x'. Blue and red plots correspond to SF and SAF free layers, respectively.

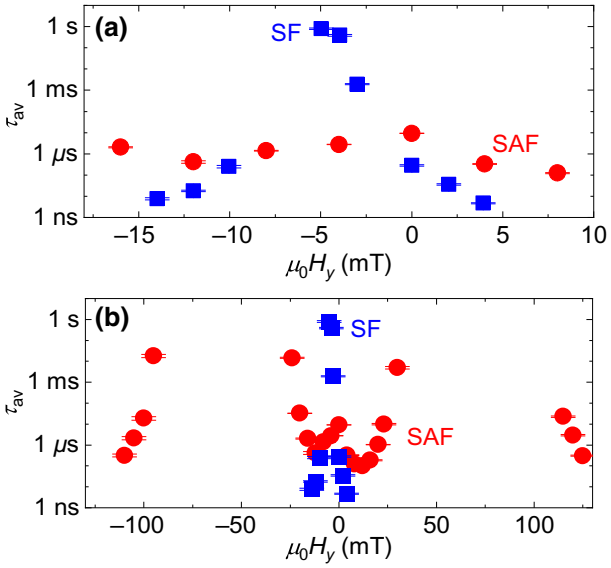

FIG. 4. Average relaxation time, τ_{av}, as a function of y-direction magnetic field, $\mu_0 H_y$, in the range of (a) ±15 mT and (b) ±130 mT. Blue and red plots denote SF free layer and SAF free layer, respectively.

SAF free layer against H_y compared with the case of H_x. Furthermore, in Fig. 4(b), we find that, over a wider range, the overall trend of τ_{av} versus H_y is distinct between the two structures: the SF free layer shows only one prominent peak at $\mu_0 H_y = -5$ mT, whereas the SAF free layer shows two prominent peaks at $\mu_0 H_y \approx \pm 70$ mT and one more small peak at $\mu_0 H_y = 0$ mT. In the SF free layer, there are no peaks at $\mu_0 |H_y| > 15$ mT, since magnetization is fixed in the y direction in this range.

III. CALCULATION

In Sec. II, we experimentally show that the SAF free layer has robust properties against magnetic fields in the x and y directions. However, even for the SAF free layer, much smaller but finite variations of the properties under H_x and H_y are observed. In addition, the SF and SAF free layers are shown to have distinct τ_{av} versus H_y trends. In this section, the magnetostatic and dynamic magnetization-reversal properties of the SAF-free-layer MTJs are investigated using a macrospin model with analytical formulas and numerical simulations, respectively.

A. Static process

For the elliptical SAF free layer with in-plane magnetization shown in Fig. 5(a), the total energy can be expressed by Eq. (1) by considering the magnetic anisotropy energy, the coupling energy of the RKKY interaction, and the Zeeman energy. Note that we assume a quasi-static process

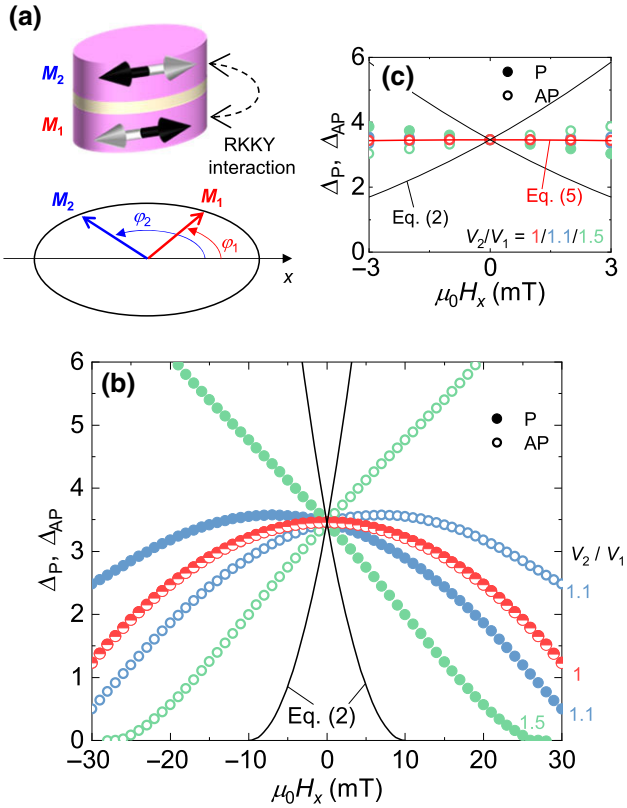

FIG. 5. (a) Schematic of SAF free layer used in macrospin simulations. Thermal stability factors Δ_P and Δ_{AP} of the SAF free layer versus H_x in the range of ±30 mT (b) and ±3 mT (c) for different ratios of the volumes of two ferromagnetic layers. Following parameters are used: $M_S = 1.8$ T, $V = V_1 + V_2 = 2 \times 10^{-24}$ m^3, $\mu_0 H_{K,in} = 10$ mT, $\mu_0 H_{RKKY} = 150$ mT. Black and red curves show analytical expressions of Eq. (2) for SF free layer and Eq. (5) for SAF free layer with the same volumes, respectively.

with magnetizations confined in the film plane as

$$E = \frac{1}{2} M_S H_{K,\mathrm{in},1} V_1 \sin^2\varphi_1 + \frac{1}{2} M_S H_{K,\mathrm{in},2} V_2 \sin^2\varphi_2 + \frac{M_S H_{RKKY}(V_1 + V_2)}{4} \cos(\varphi_1 - \varphi_2) - \mathbf{M}_1 \cdot \mathbf{H} V_1 - \mathbf{M}_2 \cdot \mathbf{H} V_2, \quad (1)$$

where M_S is the spontaneous magnetization, $H_{K,\mathrm{in},i}$ is the in-plane anisotropy field of layer i (1, lower free layer; 2, upper free layer), V_i is the volume, $\mathbf{M}_i$ is the magnetization vector, $\mathbf{H}$ is the external magnetic field vector, and φ_i is the azimuthal angle from the long axis. We derive the thermal stability factor, $\Delta = E/k_B T$, under magnetic fields by calculating the energy difference, E, between minima and saddle points from Eq. (1), where k_B is the Boltzmann constant and T is the temperature.

1. Easy-axis-field (H_x) dependence

First, we describe Δ of the SF free layer under the easy-axis magnetic field, H_x. Assuming that magnetization of the reference layer beneath the tunneling barrier is fixed to the $-x$ direction, Δ for a transition from P to AP states ($\Delta_{\rm P}$) and from AP to P states ($\Delta_{\rm AP}$) quadratically vary with H_x as

$$\Delta_{\rm P(AP)} = \frac{M_S H_{K,\rm in} V}{2k_B T}\left(1 - (+)\frac{H_x}{H_{K,\rm in}}\right)^2. \tag{2}$$

The black curves in Figs. 5(b) and 5(c) show Δ of the SF free layer given from Eq. (2), where Δ without external perturbation (Δ_0) is set to be 3.5, $M_S = 1.8$ T, $\mu_0 H_{K,\rm in} = 10$ mT, and $V = 2.0 \times 10^{-24}$ m^3. $\Delta_{\rm P}$ and $\Delta_{\rm AP}$ vary by more than 3 times in the magnetic field range of ± 3 mT. The ratio and geometric mean of the relaxation times of the AP and P states can be derived from Eq. (3a) by using the Néel-Arrhenius law, $\tau_{\rm P(AP)} = \tau_0 \exp(\Delta_{\rm P(AP)})$, as

$$\frac{\tau_{\rm AP}}{\tau_{\rm P}} = \exp\left(\frac{2M_S V}{k_B T} H_x\right), \tag{3a}$$

$$\tau_{\rm av} = \sqrt{\tau_{\rm P}\tau_{\rm AP}} = \tau_0 \exp\left(\frac{\Delta_{\rm P} + \Delta_{\rm AP}}{2}\right) = \tau_0 \exp(\Delta_0). \tag{3b}$$

Equation (3a) indicates an exponential increase of $\tau_{\rm AP}/\tau_{\rm P}$ with H_x, which is in agreement with the experimental results shown in Fig. 3(b).

Next, we examine the change in Δ of the SAF free layer under H_x to clarify the mechanism of the robustness to the easy-axis magnetic field, H_x, shown in Figs. 3(a) and 3(b), and to obtain insights into the factors governing the robustness. We assume $\Delta_0 = 3.5$, $M_S = 1.8$ T, $\mu_0 H_{K,\rm in} = 10$ mT, and $V = 2 \times 10^{-24}$ m^3, which are the same values as those used to calculate the SF free layer. $\mu_0 H_{\rm RKKY}$ is set to be 150 mT, according to our experimental result shown in Fig. 1(b). Figures 5(b) and 5(c) show Δ of the SAF free layer in the range of ± 30 and ± 3 mT, respectively, calculated with Eq. (1) for different ratios between the upper and lower magnetic layers. Note that $V_2/V_1 \neq 1$ corresponds to the situation where the magnetic moments are not fully compensated. The sum of the upper and lower volumes, $V_1 + V_2$, defined as the total volume, V, is kept constant for all V_2/V_1 ratios. For the fully compensated case (red symbols), $\Delta_{\rm P} = \Delta_{\rm AP}$, i.e., $\tau_{\rm P} = \tau_{\rm AP}$, over the whole H_x range shown in Fig. 5(b), whereas for the uncompensated case (blue and green symbols), $\Delta_{\rm P}$ intersects with $\Delta_{\rm AP}$ at $H_x = 0$ as in the SF free layer, which is consistent with our experimental results, suggesting that the fabricated SAF free layer has an uncompensated moment. There is no apparent variation in $\Delta_{\rm P}$ and $\Delta_{\rm AP}$ of the SAF free layer with fully compensated magnetic moments in the small-H_x range, as shown in Fig. 5(c). Note that, even for the compensated case, $\Delta_{\rm P} = \Delta_{\rm AP}$ only when H_x satisfies the condition

$$|H_x| < H_{\rm SF} \equiv (H_{\rm RKKY} - H_{K,\rm in})\sqrt{\frac{H_{K,\rm in}}{H_{\rm RKKY} + H_{K,\rm in}}}, \tag{4}$$

where only $(\varphi_1, \varphi_2) = (0, \pi)$ and $(\pi, 0)$ are the stable points, and the magnetizations in the free layer reverse while maintaining antiferromagnetic coupling. When $|H_x|$ exceeds this threshold field, $H_{\rm SF}$, the spin-flop state $(\varphi_1, \varphi_2) = (\pm\varphi, \mp\varphi)$ becomes stable, where φ is a positive angle determined by Eq. (1), resulting in $\Delta_{\rm P} \neq \Delta_{\rm AP}$ [31, 32]. In the H_x range satisfying Eq. (4), $\Delta (= \Delta_{\rm P} = \Delta_{\rm AP})$ is described as

$$\Delta = -\frac{M_S V}{2k_B T(H_{\rm RKKY} - H_{K,\rm in})} H_x^2 + \frac{M_S H_{K,\rm in} V}{2k_B T}, \tag{5}$$

where $H_{\rm RKKY} > 2H_{K,\rm in}$ is assumed. The coefficient of ${H_x}^2$ indicates that the increase of $H_{\rm RKKY}$ decreases the effect of H_x on Δ, leading to the robustness against H_x. Because $H_{\rm RKKY} \gg H_{K,\rm in}$ is satisfied in typical in-plane SAF free layers, the contribution of the anisotropy field to the robustness is negligible. We also note that Fig. 5(c) shows virtually constant Δ for the SAF free layer within $\mu_0|H_x| < 3$ mT, which is also consistent with the result shown in Fig. 3(c), supporting the fact that our experimental condition satisfies Eq. (4).

To summarize, in the SF free layer, the thermal stability, $\Delta_{\rm P(AP)}$, significantly varies with H_x, as described in Eq. (2), because the magnetic moment is directly affected by the Zeeman energy. On the other hand, the ideal SAF free layer with $V_2/V_1 = 1$ is not affected by a Zeeman energy below $H_{\rm SF}$, resulting in $\tau_{\rm P} = \tau_{\rm AP}$. Also, even for the nonideal SAF free layer with $V_2/V_1 \neq 1$, the behavior against the external field is much mitigated because the robustness of Δ is determined by the net magnetic moment. The strength of the RKKY interaction also affects the robustness of Δ under H_x, as described in Eq. (5), since it prevents the canting of the saddle points at which the antiferromagnetic coupling of the magnetic moments is partially broken.

2. Hard-axis-field (H_y) dependence

Next, we study Δ of the SF and SAF free layers under H_y, which is found to show qualitatively different tendencies, as shown in Fig. 4. Δ of the SF free layer under H_y is described as

$$\Delta = \frac{M_S V}{2k_B T H_{K,\rm in}}(H_{K,\rm in} - |H_y|)^2. \tag{6}$$

Equation (6) represents that Δ of the SF free layer should show a single peak at $H_y = 0$ and decrease as $|H_y|$ increases

with a quadratic relationship, which agrees well with the experimental results shown in Fig. 4.

We then numerically calculate Δ of the SAF free layer under H_y from Eq. (1), as in the calculation of H_x dependence. The gray plots in Figs. 6(a) and 6(b) show the calculated H_y dependence of Δ for $V_2/V_1 = 1.0$ and 1.5, respectively, where the same parameters as those used in the calculation of Δ under H_x are assumed. For $V_2/V_1 = 1.0$, i.e., the fully compensated structure, the two prominent peaks are reproduced at $\mu_0 H_y = \pm 75$ mT [Fig. 6(a)]. Furthermore, for $V_2/V_1 = 1.5$, i.e., the uncompensated structure, the experimentally observed small peak at $\mu_0 H_y = 0$ mT is also reproduced [Fig. 6(b)]. This fact indicates that the small peak is caused by the uncompensated moment; in other words, the uncompensated SAF free layer behaves like a ferrimagnet with a finite magnetic moment, resulting in a small peak at $H_y = 0$, as in the case of the SF free layer.

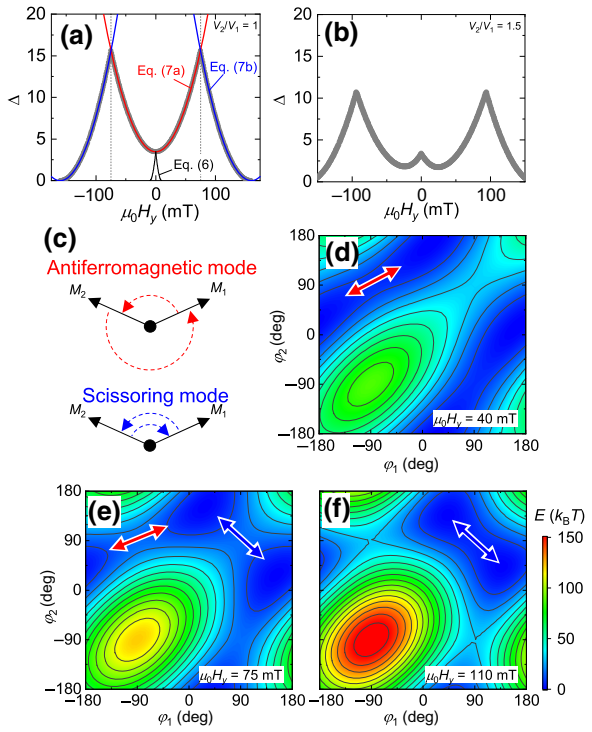

FIG. 6. Thermal stability factor versus y-direction magnetic field, H_y, for the volume ratio of $V_2/V_1 = 1.0$ (a) and $V_2/V_1 = 1.5$ (b), where $V_1 + V_2 = 2.0 \times 10^{-24}$ m^3. Gray plot shows the numerical calculations, and red and blue curves show the analytical results using Eqs. (7a) and (7b). Parameters for the simulations are the same as those used for Fig. 5. (c) Two types of magnetization-reversal mode: "antiferromagnetic mode," in which antiferromagnetic coupling is maintained, and "scissoring mode," in which magnetization reverses by breaking antiferromagnetic coupling. (d)–(f) Magnetic energy landscape at $\mu_0 H_y = 40$, 75, and 110 mT, respectively. Horizontal axis is the angle of the lower layer, and vertical axis is the angle of the upper layer in the SAF free layer.

We further investigate the H_y dependence of Δ for the fully uncompensated SAF free layer shown in Fig. 6(a), considering two different magnetization-reversal modes depicted in Fig. 6(c). Figures 6(d)–6(f) show the contour plots of the energy landscape as functions of the lower and upper free-layer angles (φ_1, φ_2) [see Fig. 5(a) for the definition] at $\mu_0 H_y = 40$, 75, and 110 mT, respectively, calculated with the same parameters as those used for Fig. 6(a). Under H_y, the stable directions of magnetizations cant towards the y direction with $\varphi_1 = \pi - \varphi_2$, which is also derived by solving E with φ_1 and φ_2 using Eq. (1). Upon increasing H_y, the switching mode transits from an antiferromagnetic mode to a scissoring mode, shown in Fig. 6(c), where magnetization switches while maintaining (breaking) antiferromagnetic coupling for the former (latter). This transition takes place at $\mu_0 H_y = \mu_0 H_{\mathrm{RKKY}}/2 = 75$ mT, as shown in Fig. 6(a). Below this critical field, the RKKY coupling energy is larger than the Zeeman energy, and the magnetic moments follow the trajectory shown by the red arrow in Fig. 6(d), i.e., the antiferromagnetic mode, where Δ is analytically expressed as

$$\Delta = \frac{M_S V}{2k_B T(H_{\mathrm{RKKY}} + H_{K,\mathrm{in}})} H_y^2 + \frac{M_S H_{K,\mathrm{in}} V}{2k_B T}. \tag{7a}$$

The red curve in Fig. 6(a) represents Eq. (7a). Above the critical field, on the other hand, the RKKY coupling energy is smaller than the Zeeman energy, and the magnetic moments follow the trajectory shown by the blue arrow in Fig. 6(f), i.e., the scissoring mode, where Δ is analytically expressed as

$$\Delta = \frac{M_S V}{2k_B T(H_{\mathrm{RKKY}} + H_{K,\mathrm{in}})} [(H_{\mathrm{RKKY}} + H_{K,\mathrm{in}}) - |H_y|]^2. \tag{7b}$$

The blue curves in Fig. 6(a) represent Eq. (7b). By considering these differences in the magnetization-reversal path, the H_y dependence of Δ can be expressed as shown in Fig. 6(b). Equations (7a) and (7b) indicate that the impact of H_y on Δ can be reduced by increasing H_{RKKY}, as with the case of the H_x dependences, since H_{RKKY}, which works to maintain the antiparallel state, prevents the canting of the stable directions of magnetic moments towards (φ, $\pi - \varphi$) under H_y.

B. Dynamic process

Finally, we calculate the magnetization dynamics of the SF and SAF free layers to discuss their robustness considering the out-of-plane degrees of freedom of the magnetization, as well as the dynamic process to switch the magnetization configuration, which is not taken into account in the quasi-static calculation described above.

The dynamics of the two antiferromagnetically coupled magnetizations are described by the LLG equation as

$$\frac{d\mathbf{M}_i}{dt} = -\gamma\mu_0[\mathbf{M}_i \times (\mathbf{H}_i + \mathbf{H}_{\mathrm{th},i})] + \alpha\left(\frac{\mathbf{M}_i}{M_S} \times \frac{d\mathbf{M}_i}{dt}\right), \tag{8}$$

where α is the damping constant, γ is the gyromagnetic ratio, $\mathbf{H}_i$ is the effective field vector ($\equiv -\partial E/\partial \mathbf{M}_i$) of free layer i [=1 (lower free layer) or 2 (upper free layer)], and $\mathbf{H}_{\mathrm{th},i}$ is the thermal field vector defined by $\langle \mathbf{H}_{\mathrm{th},i} \rangle = 0$ and $\langle (\mathbf{H}_{\mathrm{th},i})^2 \rangle = 2\alpha k_B T/\mu_0\gamma M_S V_i \Delta t$, where Δt is the time step of the numerical calculation [33]. To simulate the SAF free layer depicted in Fig. 5(a), we include the perpendicular and in-plane magnetic anisotropies by considering interfacial magnetic anisotropy and the shape magnetic anisotropy. We set $V_1 = V_2 = 1.0 \times 10^{-24}$ m^3, $\mu_0 H_{K,1}^{\mathrm{eff}} = -0.80$ T, $\mu_0 H_{K,2}^{\mathrm{eff}} = -1.8$ T, $\mu_0 H_{K,\mathrm{in},1} = \mu_0 H_{K,\mathrm{in},2} = 10$ mT, and $\mu_0 H_{\mathrm{RKKY}} = 150$ mT. Note that the effective perpendicular anisotropy fields of the lower and upper layers have different values, considering the interfacial anisotropy for the lower layer. As a reference, we simulate the magnetization dynamics of the SF free layer with the same geometry, where we set $V = 2.0 \times 10^{-24}$ m^3, which is the same as the total volume of the SAF free layer; $\mu_0 H_K^{\mathrm{eff}} = -1.3$ T; and $\mu_0 H_{K,\mathrm{in}} = 10$ mT. The damping constant and spontaneous magnetization are set to be 0.005 and 1.8 T, respectively, for all the ferromagnetic layers. All LLG simulations are conducted by using the Runge Kutta method with a time step of $\Delta t = 200$ fs, which is sufficiently small that the simulation result can be converged.

The calculated τ versus H_x results are shown in Fig. 7. The relaxation time, τ, of the SF free layer (blue symbols) changes by more than 3 times for both the P and AP states under $\mu_0 H_x = \pm 1.5$ mT, whereas, for the SAF free layer (red symbols), there are no apparent variations in τ, which is consistent with the explanation given in Sec. III A. Additionally, their relaxation times differ by 2 times, despite having the same thermal stability factor, which is not expected from the calculation based on the static process. This difference can be attributed to the following two factors related to the dynamic process, especially the variation of the attempt time [22]: (1) the effect of the perpendicular anisotropy and (2) the effective field of the RKKY coupling. Concerning (1), the perpendicular anisotropy of interacting stochastic nanomagnets with an in-plane easy axis is presumed to affect the attempt time, as reported for the noninteracting geometry that the attempt time is a power function with negative exponents β as $|H_K^{\mathrm{eff}}|^\beta$ [22]. Concerning (2), the force maintaining a stable state, i.e., the effective field of the RKKY coupling, is most likely to cause a reduction in the frequency of attempts to overcome the energy barrier, leading to an increase of the attempt time. The calculation of the dynamic process confirms the robustness of the relaxation time against magnetic fields in the SAF free layer similar to the calculation of the static process. We also find a difference in the relaxation time between SF and SAF free layers, which is not accessible in the calculation of the static process.

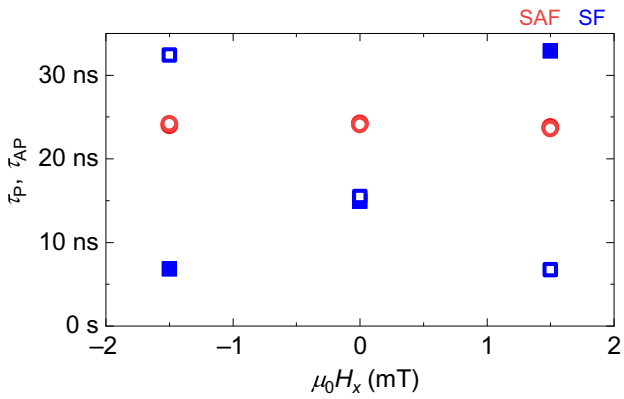

FIG. 7. Relaxation time, τ_P (τ_{AP}), of P (AP) state against the x-direction magnetic field shown by open (closed) symbols. Blue and red plots show the SF and SAF free layers, respectively.

IV. DISCUSSION

In Sec. II, we experimentally show that the relaxation time of the SAF free layer is much more robust than that of the SF free layer from the magnetic field dependence of the relaxation time against both x and y directions. In Sec. III, we theoretically study the external magnetic field dependences of Δ by calculating the quasi-static and dynamic processes. In this section, we discuss the strategy to realize external-field-robust stochastic MTJs using a SAF free layer based on these experimental and calculation results.

First, we discuss the impact of the uncompensated moment on the SAF structure. As shown in Figs. 3 and 4, in the case of the SAF structure with the uncompensated moment, H_x varies with τ_{AP}/τ_P and H_y varies with τ_{av}. Because these characteristics are not preferable for applications, compensation of the magnetic moments is the most critical factor. Accordingly, one needs to carefully consider the effects of the dead layer at the interface with the adjacent layer, the shape of the pillar of the junction, and the edge damage of each layer after the fabrication process [34–37]. In this regard, the measurement of the RTN of MTJs against H_y at around $H_y = 0$ can serve as a sensitive tool, as shown in Fig. 4.

Next, we discuss the requirements to achieve high robustness, assuming that a fully compensated SAF structure can be fabricated. In the SAF with $V_1 = V_2$, the coefficients of ${H_x}^2$ and ${H_y}^2$ of Δ in Eqs. (5), (7a), and (7b) indicate that the robustness to magnetic fields can be improved by decreasing the magnetic moment and/or by increasing the RKKY coupling. To obtain a design criterion for probabilistic computing applications, we set the

acceptable variation of the thermal stability factor, $\delta\Delta$, to suppress the variation of τ to be less than about 10% under an external magnetic field of several mT, assuming a general magnetic shielding technique for industrial use [38–41]. This condition corresponds to $\delta\Delta$ of 0.1 in the case of $V_1 = V_2 = 1.0 \times 10^{-24}$ m^3, $M_S = 1.8$ T, and $\mu_0 H_{K,\mathrm{in}} = 10$ mT ($\Delta = 3.5$). Also, comparing the coefficients of the H_x and H_y terms in Eqs. (5) and (7a), we find that Δ is always more sensitive to H_x than to H_y. Then, from Eq. (5), the required $\mu_0 H_{\mathrm{RKKY}}$ is derived to be >360 mT for $\delta\Delta < 0.1$ in the H_x range of about 10 mT. While this is about twice as large as the value obtained in our experiment, we note that the required H_{RKKY} linearly decreases with a reduction of the magnetic moment. We also note that, as can be understood from Eqs. (5) and (7a), H_{RKKY} does not affect Δ itself at around zero field. Therefore, the material and thickness of the nonmagnetic layer between the two free layers is a critical factor in designing robust stochastic MTJs with the SAF free layer.

V. CONCLUSION

Here, we fabricate stochastic magnetic tunnel junctions with a synthetic antiferromagnetic free layer and investigate their relaxation times as a function of external magnetic fields. Much more robust relaxation times are experimentally confirmed in the synthetic antiferromagnetic free layer than that of a single ferromagnetic free layer under in-plane magnetic fields with both easy- (x) and hard- (y) axis directions. We calculate the variation of the thermal stability factor with external magnetic fields H_x and H_y by macrospin simulation. We find that, in the case of the fully compensated synthetic antiferromagnetic free layers, the thermal stability factors for parallel and antiparallel configurations are equivalent over a range where the RKKY interaction is larger than external field H_x. The dependence on H_y is different from that of the single ferromagnetic free layer, and we reproduce this tendency by considering the magnetization-reversal mechanism. These calculation results reveal that the magnetic field robustness can be improved by decreasing the magnetic moment of each free layer and increasing the RKKY interaction. This work experimentally and analytically clarifies the external magnetic field robustness of stochastic magnetic tunnel junctions with a synthetic antiferromagnetic free layer and provides design guidelines for probabilistic computing applications.

ACKNOWLEDGMENTS

The authors thank B. Jinnai, C. Igarashi, I. Morita, and F. Shibata for technical support. This work is supported, in part, by the JST-CREST Grant No. JPMJCR19K3; JST-PRESTO Grant No. JPMJPR21B2; JSPS Kakenhi Grants No. 19H05622, No. 19KK0130, and No. 20H02178; NEDO Project No. JPNP20004; Shimadzu Science Foundation; and Cooperative Research Projects of RIEC. W.A.B. acknowledges JST-OPERA for financial support.

[1] B. Sutton, K. Y. Camsari, B. Behin-Aein, and S. Datta, Intrinsic optimization using stochastic nanomagnets, Sci. Rep. **7**, 44370 (2017).

[2] K. Y. Camsari, R. Faria, B. M. Sutton, and S. Datta, Stochastic p-bits for invertible logic, Phys. Rev. X **7**, 031014 (2017).

[3] A. Z. Pervaiz, L. A. Ghantasala, K. Y. Camsari, and S. Datta, Hardware emulation of stochastic p-bits for invertible logic, Sci. Rep. **7**, 10994 (2017).

[4] K. Y. Camsari, S. Salahuddin, and S. Datta, Implementing p-bits with embedded MTJ, IEEE Electron Device Lett. **38**, 1767 (2017).

[5] R. Faria, K. Y. Camsari, and S. Datta, Implementing Bayesian networks with embedded stochastic MRAM, AIP Adv. **8**, 045101 (2018).

[6] A. Mizrahi, T. Hirtzlin, A. Fukushima, H. Kubota, S. Yuasa, J. Grollier, and D. Querlioz, Neural-like computing with populations of superparamagnetic basis functions, Nat. Commun. **9**, 1533 (2018).

[7] W. A. Borders, A. Z. Pervaiz, S. Fukami, K. Y. Camsari, H. Ohno, and S. Datta, Integer factorization using stochastic magnetic tunnel junctions, Nature **573**, 390 (2019).

[8] M. W. Daniels, A. Madhavan, P. Talatchian, A. Mizrahi, and M. D. Stiles, Energy-Efficient Stochastic Computing with Superparamagnetic Tunnel Junctions, Phys. Rev. Appl. **13**, 034016 (2020).

[9] P. Debashis, V. Ostwal, R. Faria, S. Datta, J. Appenzeller, and Z. Chen, Hardware implementation of Bayesian network building blocks with stochastic spintronic devices, Sci. Rep. **10**, 16002 (2020).

[10] Y. Shao, S. L. Sinaga, I. O. Sunmola, A. S. Borland, M. J. Carey, J. A. Katine, V. Lopez-Dominguez, and P. K. Amiri, Implementation of artificial neural networks using magnetoresistive random-access memory-based stochastic computing units, IEEE Magn. Lett. **12**, 4501005 (2021).

[11] J. Kaiser and S. Datta, Probabilistic computing with p-bits, Appl. Phys. Lett. **119**, 150503 (2021).

[12] J. Kaiser, W. A. Borders, K. Y. Camsari, S. Fukami, H. Ohno, and S. Datta, Hardware-Aware *In Situ* Learning Based on Stochastic Magnetic Tunnel Junctions, Phys. Rev. Appl. **17**, 014016 (2022).

[13] A. Grimaldi, L. Sánchez-Tejerina, N. Anjum Aadit, S. Chiappini, M. Carpentieri, K. Camsari, and G. Finocchio, Spintronics-Compatible Approach to Solving Maximum-Satisfiability Problems with Probabilistic Computing, Invertible Logic, and Parallel Tempering, Phys. Rev. Appl. **17**, 024052 (2022).

[14] D. Vodenicarevic, N. Locatelli, A. Mizrahi, J. S. Friedman, A. F. Vincent, M. Romera, A. Fukushima, K. Yakushiji, H. Kubota, S. Yuasa, *et al.*, Low-Energy Truly Random Number Generation with Superparamagnetic Tunnel Junctions for Unconventional Computing, Phys. Rev. Appl. **8**, 054045 (2017).

[15] M. Bapna and S. A. Majetich, Current control of time-averaged magnetization in superparamagnetic tunnel junctions, Appl. Phys. Lett. **111**, 243107 (2017).
[16] C. M. Liyanagedera, A. Sengupta, A. Jaiswal, and K. Roy, Stochastic Spiking Neural Networks Enabled by Magnetic Tunnel Junctions: From Nontelegraphic to Telegraphic Switching Regimes, Phys. Rev. Appl. **8**, 064017 (2017).
[17] B. Parks, M. Bapna, J. Igbokwe, H. Almasi, W. Wang, and S. A. Majetich, Superparamagnetic perpendicular magnetic tunnel junctions for true random number generators, AIP Adv. **8**, 055903 (2018).
[18] J. Cai, B. Fang, L. Zhang, W. Lv, B. Zhang, T. Zhou, G. Finocchio, and Z. Zeng, Voltage-Controlled Spintronic Stochastic Neuron Based on a Magnetic Tunnel Junction, Phys. Rev. Appl. **11**, 034015 (2019).
[19] V. Ostwal and J. Appenzeller, Spin–orbit torque-controlled magnetic tunnel junction with low thermal stability for tunable random number generation, IEEE Magn. Lett. **10**, 4503305 (2019).
[20] J. Kaiser, A. Rustagi, K. Y. Camsari, J. Z. Sun, S. Datta, and P. Upadhyaya, Subnanosecond Fluctuations in Low-Barrier Nanomagnets, Phys. Rev. Appl. **12**, 054056 (2019).
[21] B. Parks, A. Abdelgawad, T. Wong, R. F. L. Evans, and S. A. Majetich, Magnetoresistance Dynamics in Superparamagnetic Co-Fe-B Nanodots, Phys. Rev. Appl. **13**, 014063 (2020).
[22] S. Kanai, K. Hayakawa, H. Ohno, and S. Fukami, Theory of relaxation time of stochastic nanomagnets, Phys. Rev. B **103**, 094423 (2021).
[23] K. Hayakawa, S. Kanai, T. Funatsu, J. Igarashi, B. Jinnai, W. A. Borders, H. Ohno, and S. Fukami, Nanosecond Random Telegraph Noise in In-Plane Magnetic Tunnel Junctions, Phys. Rev. Lett. **126**, 117202 (2021).
[24] C. Safranski, J. Kaiser, P. Trouilloud, P. Hashemi, G. Hu, and J. Z. Sun, Demonstration of nanosecond operation in stochastic magnetic tunnel junctions, Nano Lett. **21**, 2040 (2021).
[25] O. Hassan, S. Datta, and K. Y. Camsari, Quantitative Evaluation of Hardware Binary Stochastic Neurons, Phys. Rev. Appl. **15**, 064046 (2021).
[26] K. Kobayashi, W. A. Borders, S. Kanai, K. Hayakawa, H. Ohno, and S. Fukami, Sigmoidal curves of stochastic magnetic tunnel junctions with perpendicular easy axis, Appl. Phys. Lett. **119**, 132406 (2021).
[27] P. Talatchian, M. W. Daniels, A. Madhavan, M. R. Pufall, E. Jué, W. H. Rippard, J. J. McClelland, and M. D. Stiles, Mutual control of stochastic switching for two electrically coupled superparamagnetic tunnel junctions, Phys. Rev. B **104**, 054427 (2021).
[28] T. Funatsu, S. Kanai, J. Ieda, S. Fukami, and H. Ohno, Local bifurcation with spin-transfer torque in superparamagnetic tunnel junctions, Nat. Commun. **13**, 4079 (2022).
[29] S. Ikeda, H. Sato, M. Yamanouchi, H. Gan, K. Miura, K. Mizunuma, S. Kanai, S. Fukami, F. Matsukura, N. Kasai, *et al.*, Recent progress of perpendicular anisotropy magnetic tunnel junctions for nonvolatile VLSI, SPIN **02**, 1240003 (2012).
[30] W. Rippard, R. Heindl, M. Pufall, S. Russek, and A. Kos, Thermal relaxation rates of magnetic nanoparticles in the presence of magnetic fields and spin-transfer effects, Phys. Rev. B **84**, 064439 (2011).
[31] D. C. Worledge, Magnetic phase diagram of two identical coupled nanomagnets, Appl. Phys. Lett. **84**, 2847 (2004).
[32] D. C. Worledge, Spin flop switching for magnetic random access memory, Appl. Phys. Lett. **84**, 4559 (2004).
[33] W. F. Brown, Thermal fluctuations of a single-domain particle, Phys. Rev. **130**, 1677 (1963).
[34] J. M. Shaw, S. E. Russek, T. Thomson, M. J. Donahue, B. D. Terris, O. Hellwig, E. Dobisz, and M. L. Schneider, Reversal mechanisms in perpendicularly magnetized nanostructures, Phys. Rev. B **78**, 024414 (2008).
[35] J. Igarashi, J. Llandro, H. Sato, F. Matsukura, and H. Ohno, Magnetic-field-angle dependence of coercivity in CoFeB/MgO magnetic tunnel junctions with perpendicular easy axis, Appl. Phys. Lett. **111**, 132407 (2017).
[36] L. Thomas, G. Jan, S. Le, S. Serrano-Guisan, Y.-J. Lee, H. Liu, J. Zhu, J. Iwata-Harms, R. Tong, S. J. Patel, *et al.*, in *2017 IEEE International Electron Devices Meeting (IEDM)* (IEEE, San Francisco, CA, 2017), pp. 38.4.1–38.4.4.
[37] M. Shinozaki, J. Igarashi, H. Sato, and H. Ohno, Free-layer size dependence of anisotropy field in nanoscale CoFeB/MgO magnetic tunnel junctions, Appl. Phys. Express **11**, 043001 (2018).
[38] W. DeBonte and A. Butherus, Magnetically permeable adhesives and adhesive-joined shield structures, IEEE Trans. Magn. **13**, 1376 (1977).
[39] D. Apalkov, A. Khvalkovskiy, S. Watts, V. Nikitin, X. Tang, D. Lottis, K. Moon, X. Luo, E. Chen, A. Ong, *et al.*, Spin-transfer torque magnetic random access memory (STT-MRAM), J. Emerging Technol. Comput. Syst. **9**, 1 (2013).
[40] T. Watanabe and S. Yamamichi, in *2012 IEEE 62nd Electronic Components and Technology Conference* (IEEE, San Diego, CA, USA, 2012), pp. 920–925.
[41] L. T. Guan, E. W. L. Ching, L. W. Yi, T.-C. Cheng, K. Lee, J. Janesky, and E. Gow, in *2018 IEEE 20th Electronics Packaging Technology Conference (EPTC)* (IEEE, Singapore, Singapore, 2018), pp. 349–354.